SUPPLEMENTAL INFORMATION

Figure S1. Domain collection, protein expression and network analysis.
A. Signal peptide and transmembrane helix analysis of the *C. elegans* proteome (WS252 release) shows that 23% of proteins have predicted signal peptides, and 44% of proteins are either membrane-anchored or secreted.
B-E. Expression testing of *D. melanogaster* (blue) and *C. elegans* (green) ectodomains in S2 cells using the Metallothionein (MT) and Actin 5C (Ac) promoters. Rst D1 refers to the fist immunoglobulin domain of Rst. For MT-driven expression, transiently transfected cells were induced with 0.8 mM $CuSO_4$ at 16 hours post-transfection. All transfections were collected 88 hours post-transfection for western blotting using a mouse primary anti-His antibody (1:2000) and an Alexa Fluor 488-coupled donkey anti-mouse IgG secondary antibody (1:5000). Overall, the Actin 5C promoter results in higher expression, but not in every case.
F. Network of 185 interactions detected with a cutoff of $z_{min} > 8.4$ drawn using the organic layout algorithm in Cytoscape, where node size relates to node degree (see the legend), and the edge thickness scales to z_{min}.
G. The degree distribution of all the interactions depicted in F.

Figure S2. MaxEnt model to filter the experimental data.
A. The normalized experimental data An.
B. The mean of the statistical background model P.
C. The difference between An and P. PPIs with z-score above intermediate (orange) and stringent (purple) thresholds are shown in matrix form. Reciprocal PPIs are marked with dots (•) and non-reciprocal PPIs are marked with an '×'.
D. The reciprocal ratio of interactions as a function of the chosen threshold of *z*-scores. The maximum reciprocal ratio is achieved with $z = 12.2$.
E. The reciprocal ratio as a function of the number of unique edges identified. The shading represents $n \pm SE$, where *n* is the number of reciprocal edges. SE is calculated by the shot noise as $SE = \sqrt{n}$.

Figure S3. Interactions of axon guidance receptors and cues.
A. Image of the 384-well plate and absorbance at 650 nm for the ECIA experiment for selected axon guidance-related proteins in Figure 3B.
B. ECIA experiment for other guidance-related proteins. *D. melanogaster* Rst is a homodimeric protein and serves as a control.

Figure S4. The ZIG-insulin interactome.
A. Sequence alignment of four ZIGs and the fly ortholog, ImpL2. ZIG-2 to -5 carry a disulfide unique to all worm ZIGs.
B. The ECIA construct design where ZIGs are depicted as bait and insulins as prey, as used in the experiment presented in Figure 4B.
C, D. Expression of all insulin and ZIG constructs used in the experiment presented in Figure 4B. Expression of bait is shown in C and expression of prey in D.
E. Kinetic fitting of SPR sensorgrams from Figure 4D with parameters.
F. Superposition of three ZIG-4–INS-6 structures solved using three different crystal forms.

G. The INS-6–ZIG-4 complex is compatible with insulins interacting with the L1 domains + αCT helix in insulin receptors. hIR: human insulin receptor; PDB ID: 3W11.
H. Structure of the active T-like IR_2-$insulin_4$ structure from PDB ID: 6PXV. Four insulin-binding sites are shown in red, yellow, blue and pink.
I, J. Insulin-bound ZIG-4 would severely clash with dimeric IR, regardless of insulin binding to site 1 (I), or site 2 (J).

Figure S5. Comparison of AlphaFold models of complexes discovered by the ECIA screen with the structure of human ligand-bound neurotrophin receptor.
A. Structure of human neurotrophin receptor, TrkB (domain 5) bound to NT4/5 (PDB: 1HCF).
B. AlphaFold-predicted TRK-1 ectodomain bound to ZK856.6 at a 2:2 stoichiometry.
C. AlphaFold-predicted TRK-1 ectodomain bound to B0416.2 at a 2:2 stoichiometry.
D. PAE (Predicted Aligned Error) plots corresponding to models shown in B. and C. High ipTM (interface predicted Template Modelling) scores indicate high-confidence predictions.
E. Kinetic fitting of SPR sensorgrams collected for the binding of B0222.11 to HIR-1, shown in Figure 5C.

Figure S6. Interfaces observed in AlphaFold models of RIG-5-NLR-1 and RIG-5-PTP-3 complexes.
A. The AlphaFold-predicted interface of RIG-5 (ECD) bound to NLR-1 (D6).
B. The AlphaFold-predicted interface of RIG-5 (ECD) bound to PTP-3 (FN4-6). The RIG-5 residues mutated in the experiment presented in Figure 6H are shown in light cyan in A and B.

Figure S7. Binding experiments for NLG-1–NRX-1 complex.
A. SPR sensorgrams for soluble NRX-1 LNS6 domain binding to immobilized NLG-1 ECD.
B. Binding isotherm and K_D for binding shown in A.
C. Size-exclusion chromatography runs for NRX-1 LNS-6 (orange), NLG-1 ECD (green) and the mixed sample (black).

Table S1. Excel file containing even more data too large to fit in a PDF.
Ectodomains used in the interactome study by gene, transcript and protein names, sequence, domain composition, signal peptide and membrane anchoring predictions. TM: transmembrane. Relative expression levels are measured and reported in columns P and Q for bait and prey constructs, respectively.

Table S2. Excel file containing even more data too large to fit in a PDF.
A. Symmetrized *z*-scores using the MaxEnt method.
B. Asymmetric *z*-scores using the MaxEnt method.

Table S3. Excel file containing even more data too large to fit in a PDF.
List of interactions observed in the high-throughout ECIA experiment using our new MaxEnt method with 2-hour absorbance measurements. Interactions with only one orientation with $z>3$ are labeled pink in column G. For comparison, scoring according to our old method, geometric mean of trimmed z-scores ($\sqrt{(z_1 \times z_2)_{old}}$) (Özkan, et al. *Cell*, 2013), are given in H, where a score of >20 was considered significant. Column I reports if the interaction or an orthologous one was

reported before, based on a literature search. Alphafold-multimer (Colabfold version 1.5.2) iPTM scores for a subset of interacting pairs are in column J.

Table S4. Excel file containing even more data too large to fit in a PDF.
A. Canonical neighbors for every ectodomain tested, protein/sequence names in top row in bold.
B. All neighbors for every ectodomain tested, protein/sequence names in top row in bold.

Table S5. Data and refinement statistics for x-ray crystallography of the ZIG-4–INS-6 complex.

Table S6. Excel file containing even more data too large to fit in a PDF.
Experimental details and parameters for all surface plasmon experiments included in the manuscript. Biacore chips are purchased from Cytiva. HBSp+: 10 mM HEPES, 150 mM NaCl, 0.05% Tween-20.

Table S7. Excel file containing even more data too large to fit in a PDF.
185 experimental PPIs based on the number of chemical synapses associated with each interaction. Interactions where there was no expression data for one or both of the binding partners are labeled N/A. We randomize the neuron connectome as a random control.

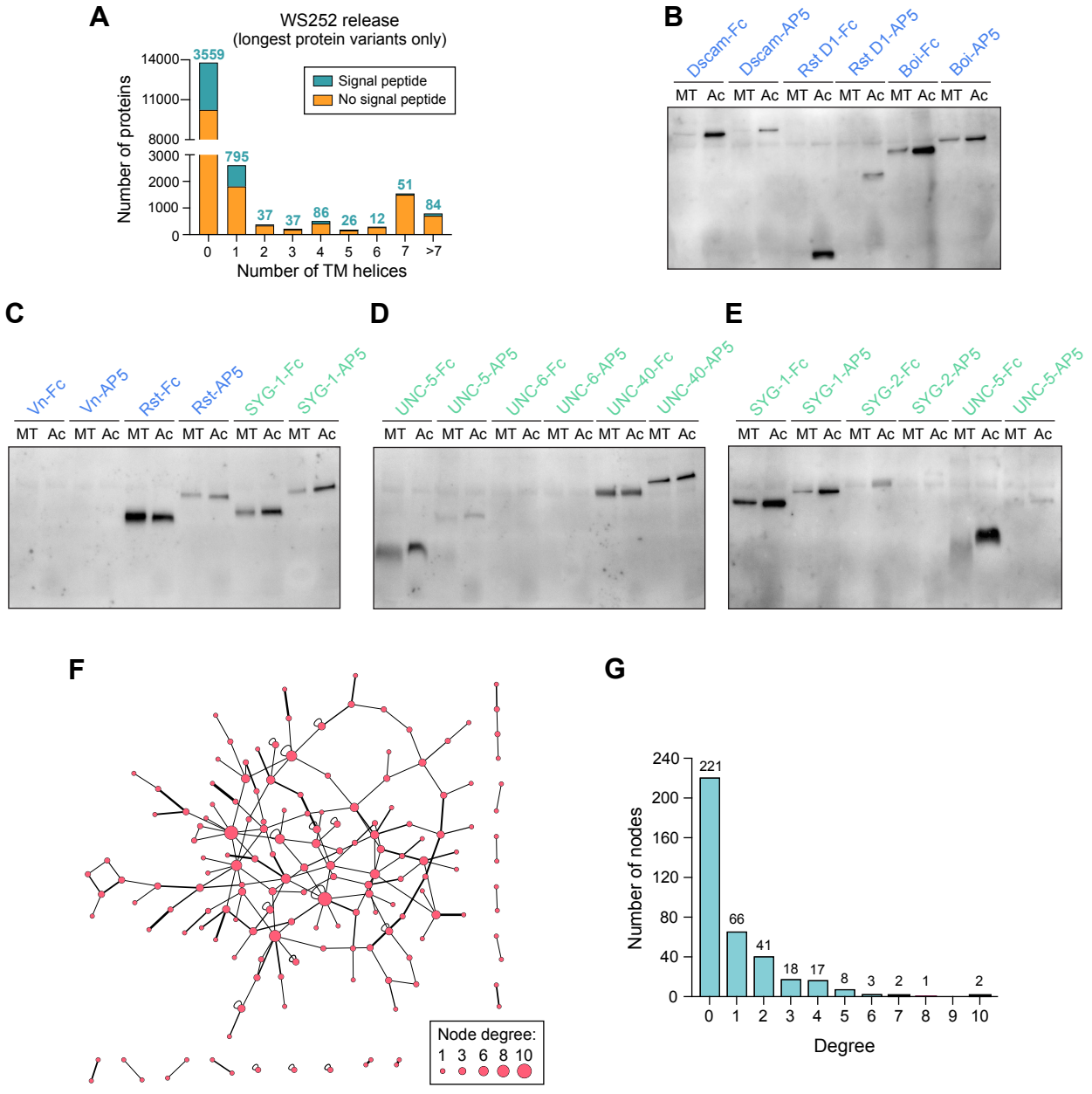

Figure S1. Domain collection, protein expression and network analysis.
A. Signal peptide and transmembrane helix analysis of the *C. elegans* proteome (WS252 release) shows that 23% of proteins have predicted signal peptides, and 44% of proteins are either membrane-anchored or secreted.
B-E. Expression testing of *D. melanogaster* (blue) and *C. elegans* (green) ectodomains in S2 cells using the Metallothionein (MT) and Actin 5C (Ac) promoters. Rst D1 refers to the fist immunoglobulin domain of Rst. For MT-driven expression, transiently transfected cells were induced with 0.8 mM $CuSO_4$ at 16 hours post-transfection. All transfections were collected 88 hours post-transfection for western blotting using a mouse primary anti-His antibody (1:2000) and an Alexa Fluor 488-coupled donkey anti-mouse IgG secondary antibody (1:5000). Overall, the Actin 5C promoter results in higher expression, but not in every case.
F. Network of 185 interactions detected with a cutoff of $z_{min} > 8.4$ drawn using the organic layout algorithm in Cytoscape, where node size relates to node degree (see the legend), and the edge thickness scales to z_{min}.
G. The degree distribution of all the interactions depicted in F.

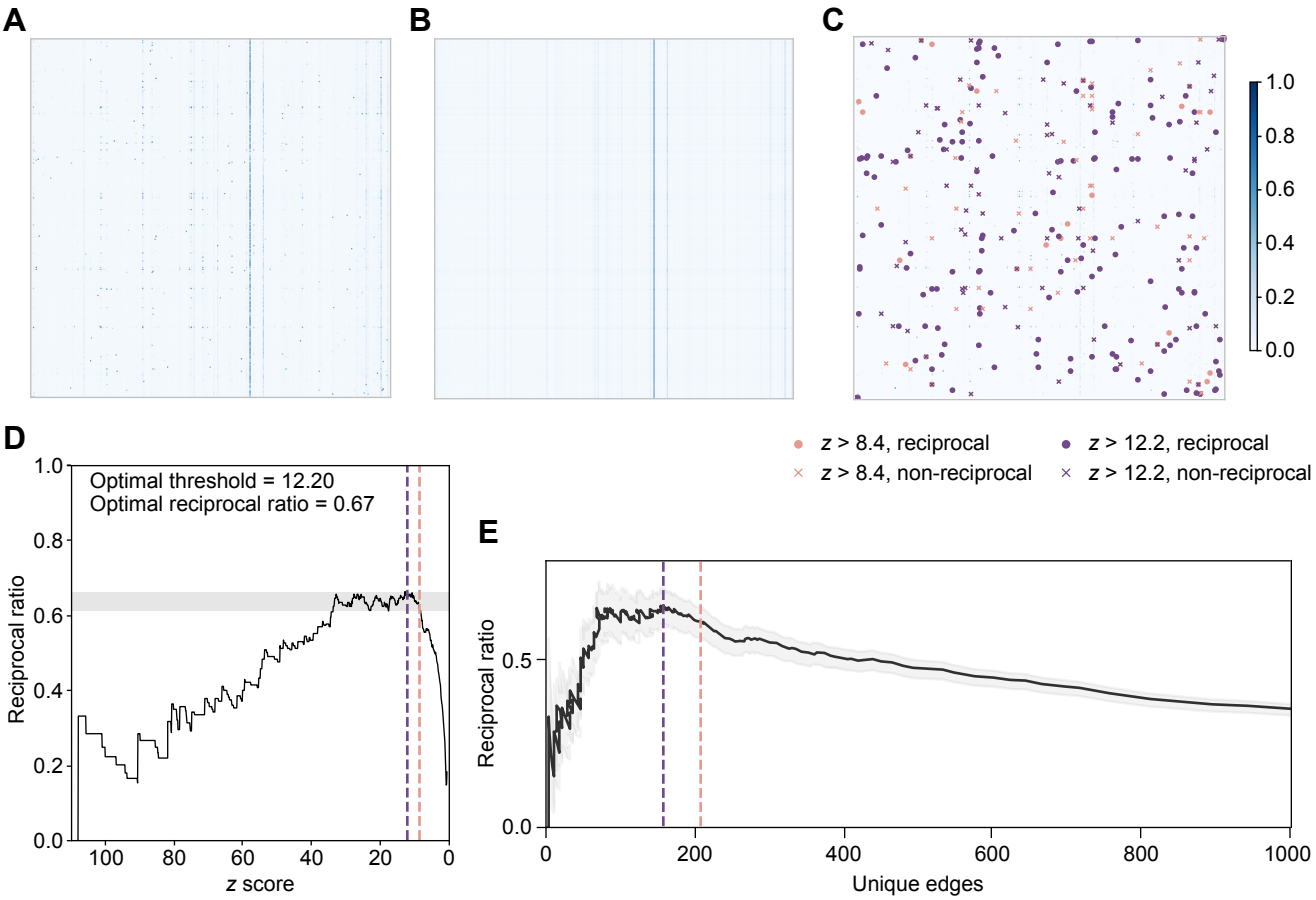

Figure S2. MaxEnt model to filter the experimental data.
A. The normalized experimental data An.
B. The mean of the statistical background model P.
C. The difference between An and P. PPIs with *z*-score above intermediate (orange) and stringent (purple) thresholds are shown in matrix form. Reciprocal PPIs are marked with dots (•) and non-reciprocal PPIs are marked with an '×'.
D. The reciprocal ratio of interactions as a function of the chosen threshold of *z*-scores. The maximum reciprocal ratio is achieved with $z = 12.2$.
E. The reciprocal ratio as a function of the number of unique edges identified. The shading represents $n \pm SE$, where n is the number of reciprocal edges. SE is calculated by the shot noise as $SE = \sqrt{n}$.

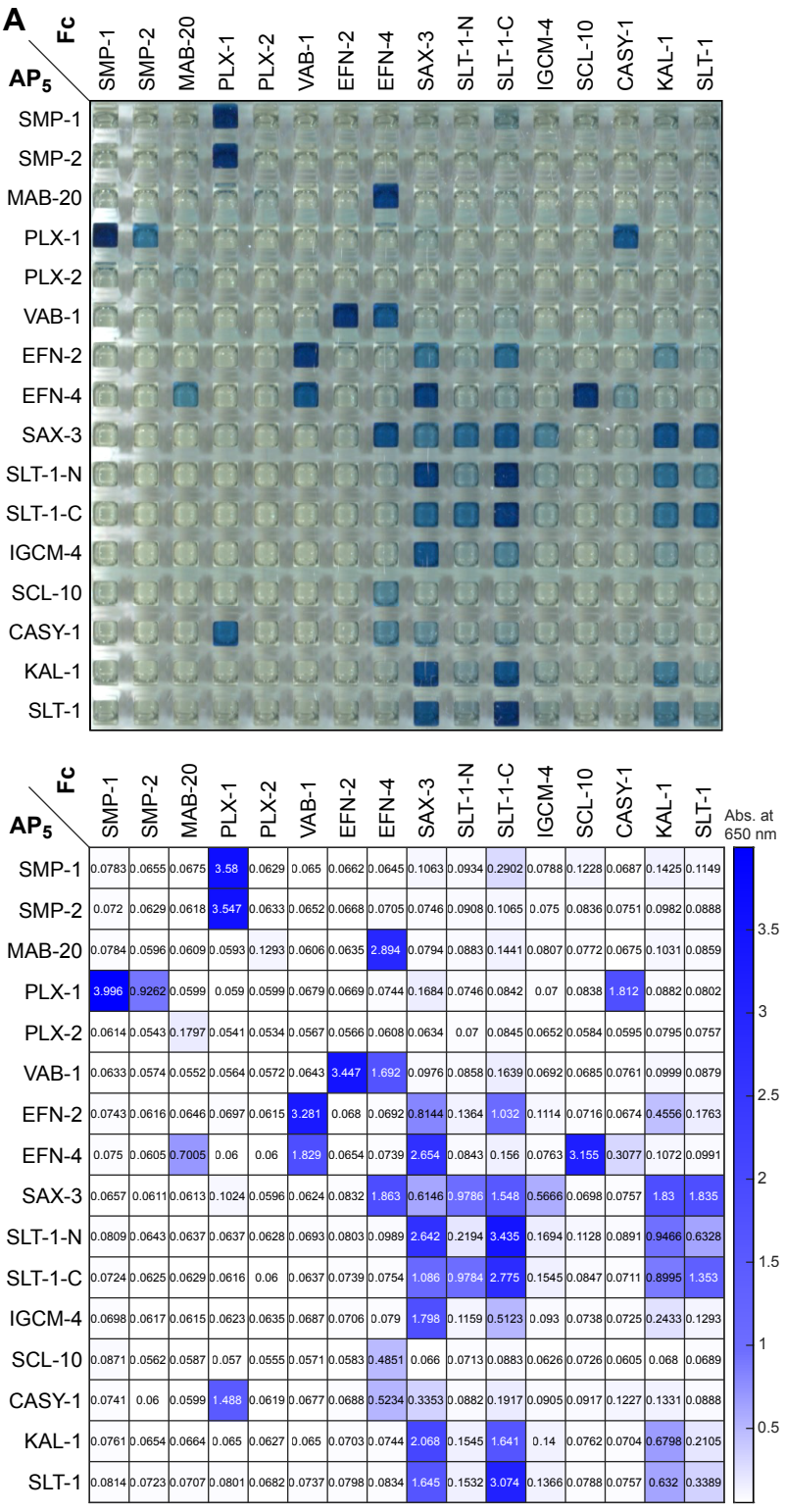

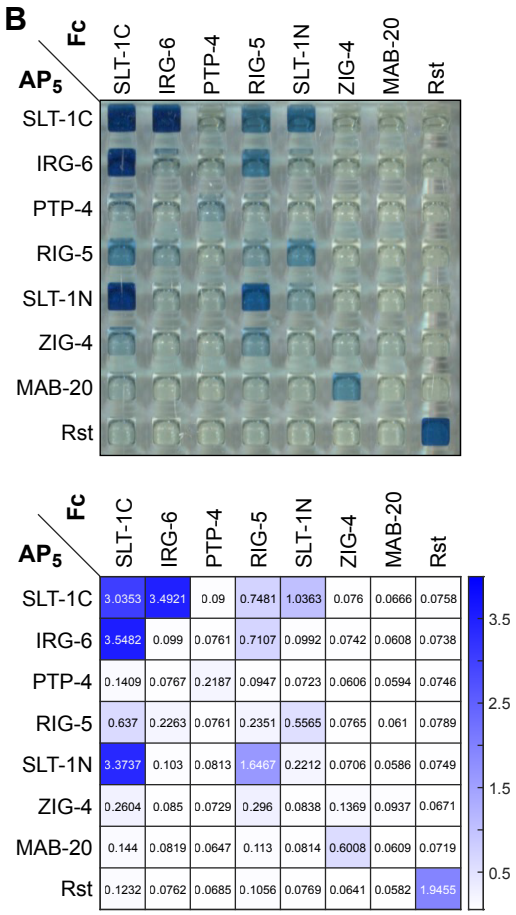

Figure S3. Interactions of axon guidance receptors and cues.
A. Image of the 384-well plate and absorbance at 650 nm for the ECIA experiment for selected axon guidance-related proteins in Figure 3B.
B. ECIA experiment for other guidance-related proteins. *D. melanogaster* Rst is a homodimeric protein and serves as a control.

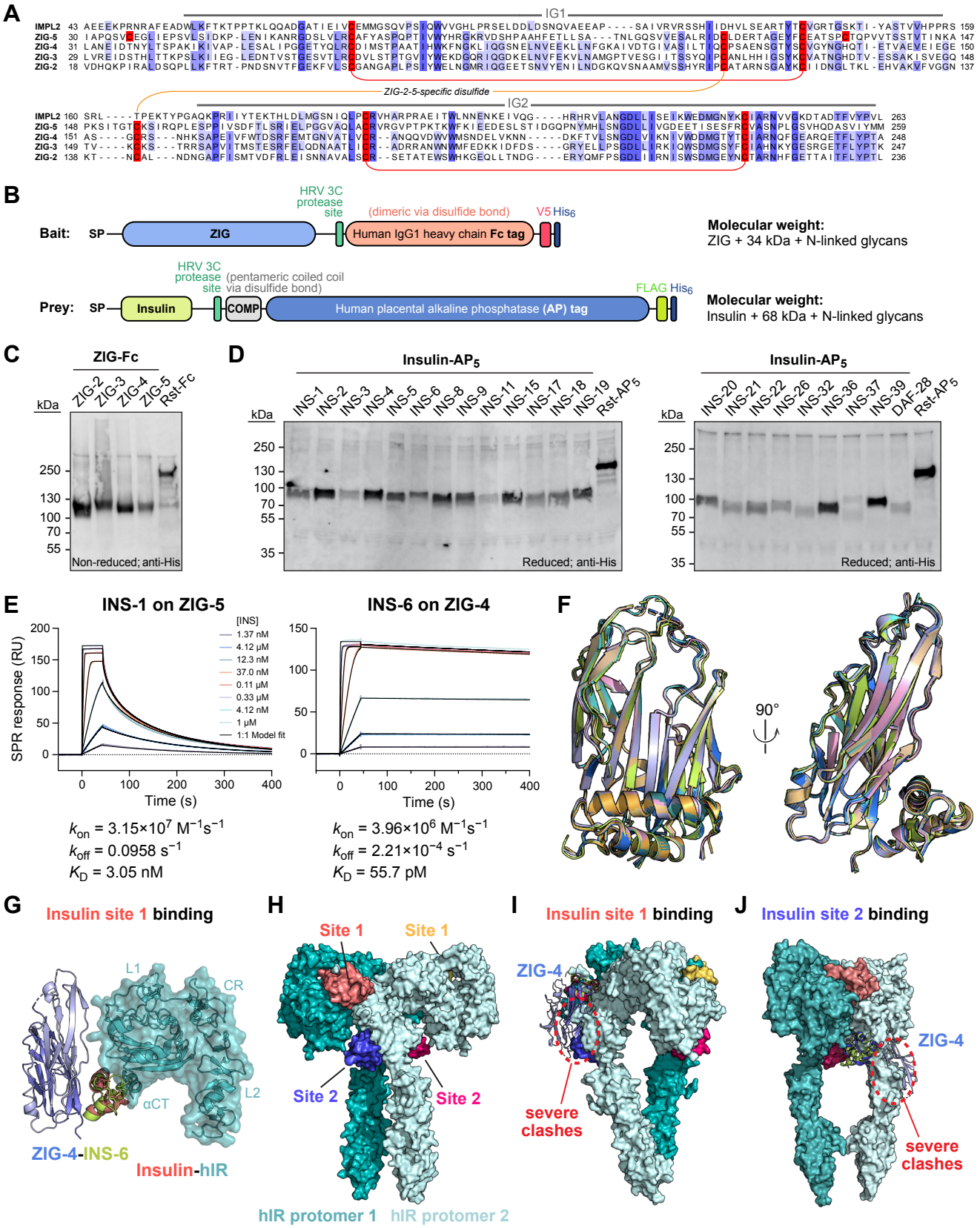

Figure S4. The ZIG-insulin interactome.

A. Sequence alignment of four ZIGs and the fly ortholog, ImpL2. ZIG-2 to -5 carry a disulfide unique to all worm ZIGs.

(continued)

(continued)
B. The ECIA construct design where ZIGs are depicted as bait and insulins as prey, as used in the experiment presented in Figure 4B.
C, D. Expression of all insulin and ZIG constructs used in the experiment presented in Figure 4B. Expression of bait is shown in C and expression of prey in D.
E. Kinetic fitting of SPR sensorgrams from Figure 4D with parameters.
F. Superposition of three ZIG-4–INS-6 structures solved using three different crystal forms.
G. The INS-6–ZIG-4 complex is compatible with insulins interacting with the L1 domains + αCT helix in insulin receptors. hIR: human insulin receptor; PDB ID: 3W11.
H. Structure of the active T-like IR_2-$insulin_4$ structure from PDB ID: 6PXV. Four insulin-binding sites are shown in red, yellow, blue and pink.
I, J. Insulin-bound ZIG-4 would severely clash with dimeric IR, regardless of insulin binding to site 1 (I), or site 2 (J).

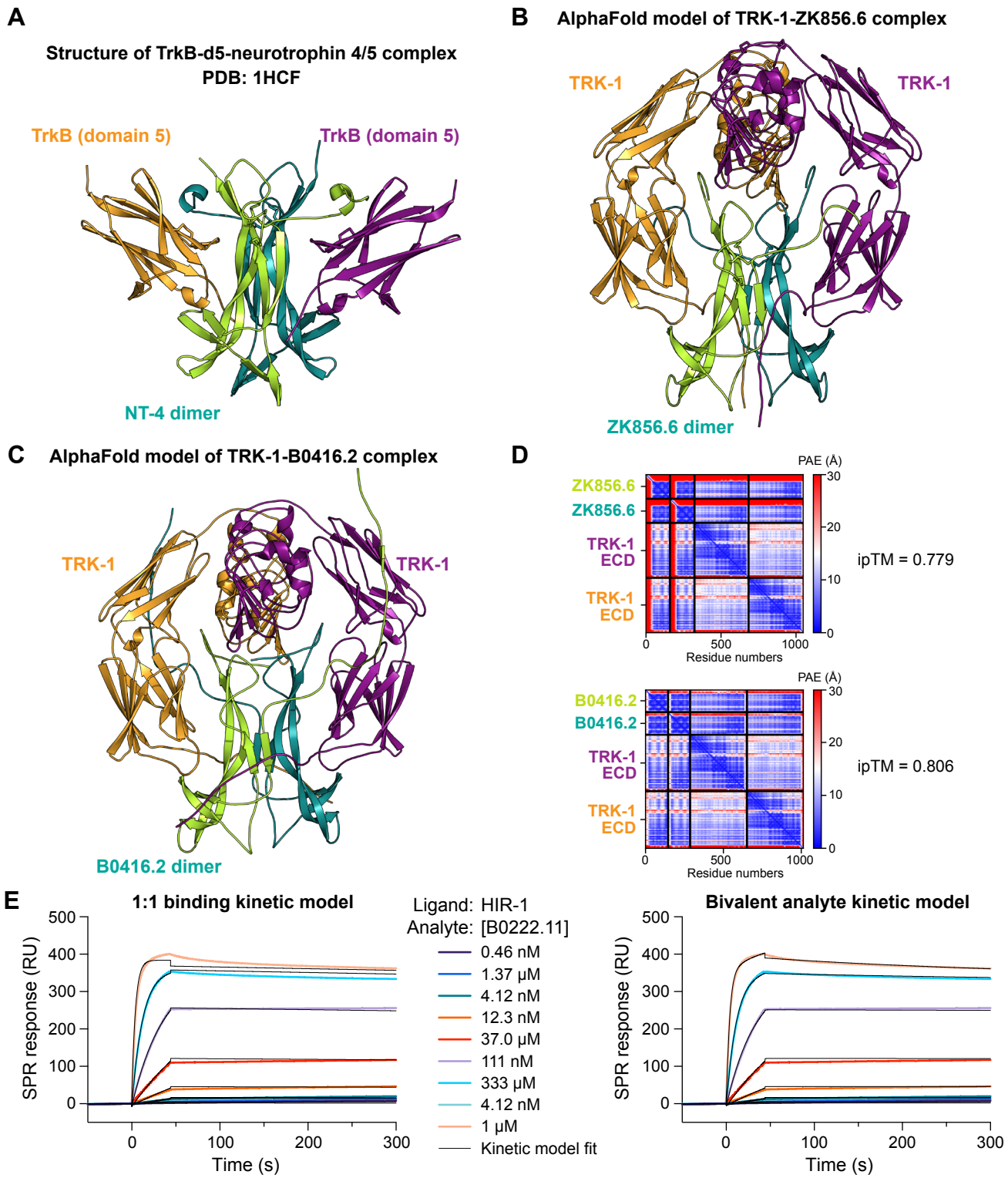

Figure S5. Comparison of AlphaFold models of complexes discovered by the ECIA screen with the structure of human ligand-bound neurotrophin receptor.
A. Structure of human neurotrophin receptor, TrkB (domain 5) bound to NT4/5 (PDB: 1HCF).
B. AlphaFold-predicted TRK-1 ectodomain bound to ZK856.6 at a 2:2 stoichiometry.
C. AlphaFold-predicted TRK-1 ectodomain bound to B0416.2 at a 2:2 stoichiometry.
D. PAE (Predicted Aligned Error) plots corresponding to models shown in B. and C. High ipTM (interface predicted Template Modelling) scores indicate high-confidence predictions.
E. Kinetic fitting of SPR sensorgrams collected for the binding of B0222.11 to HIR-1, shown in Figure 5C.

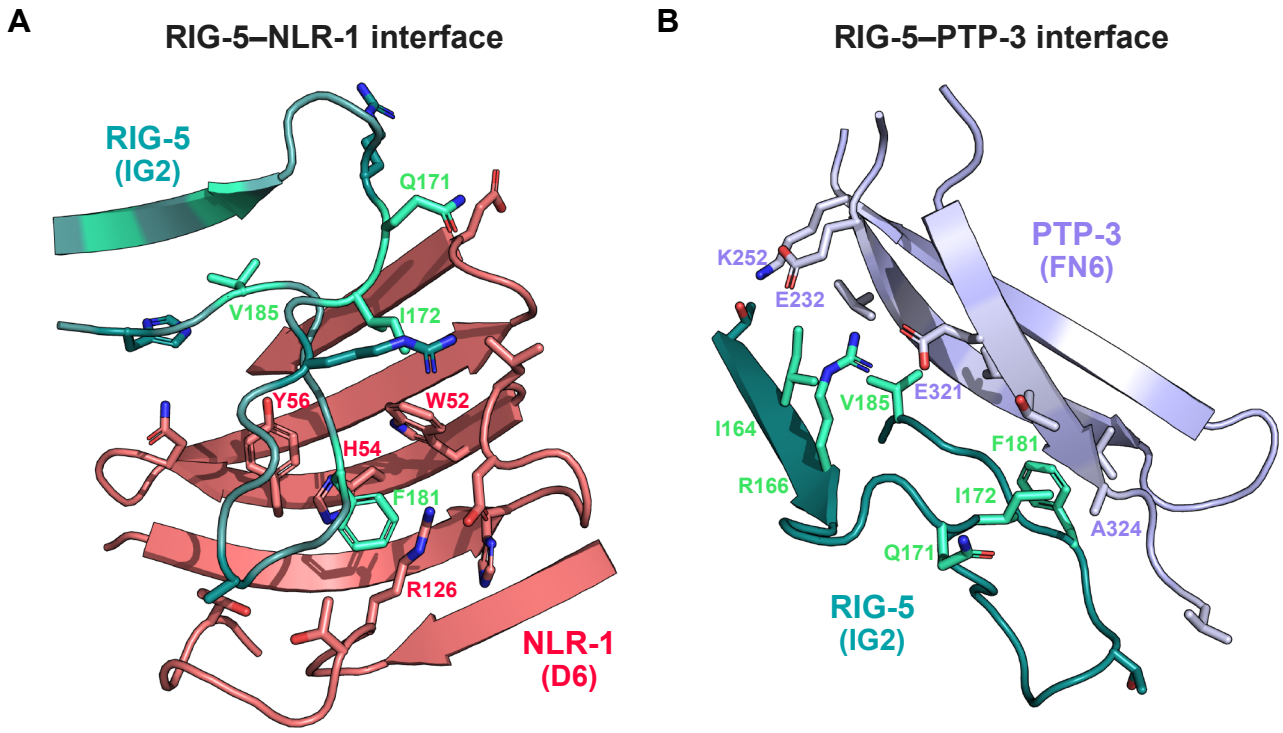

Figure S6. Interfaces observed in AlphaFold models of RIG-5-NLR-1 and RIG-5-PTP-3 complexes.
A. The AlphaFold-predicted interface of RIG-5 (ECD) bound to NLR-1 (D6).
B. The AlphaFold-predicted interface of RIG-5 (ECD) bound to PTP-3 (FN4-6). The RIG-5 residues mutated in the experiment presented in Figure 6H are shown in light cyan in A and B.

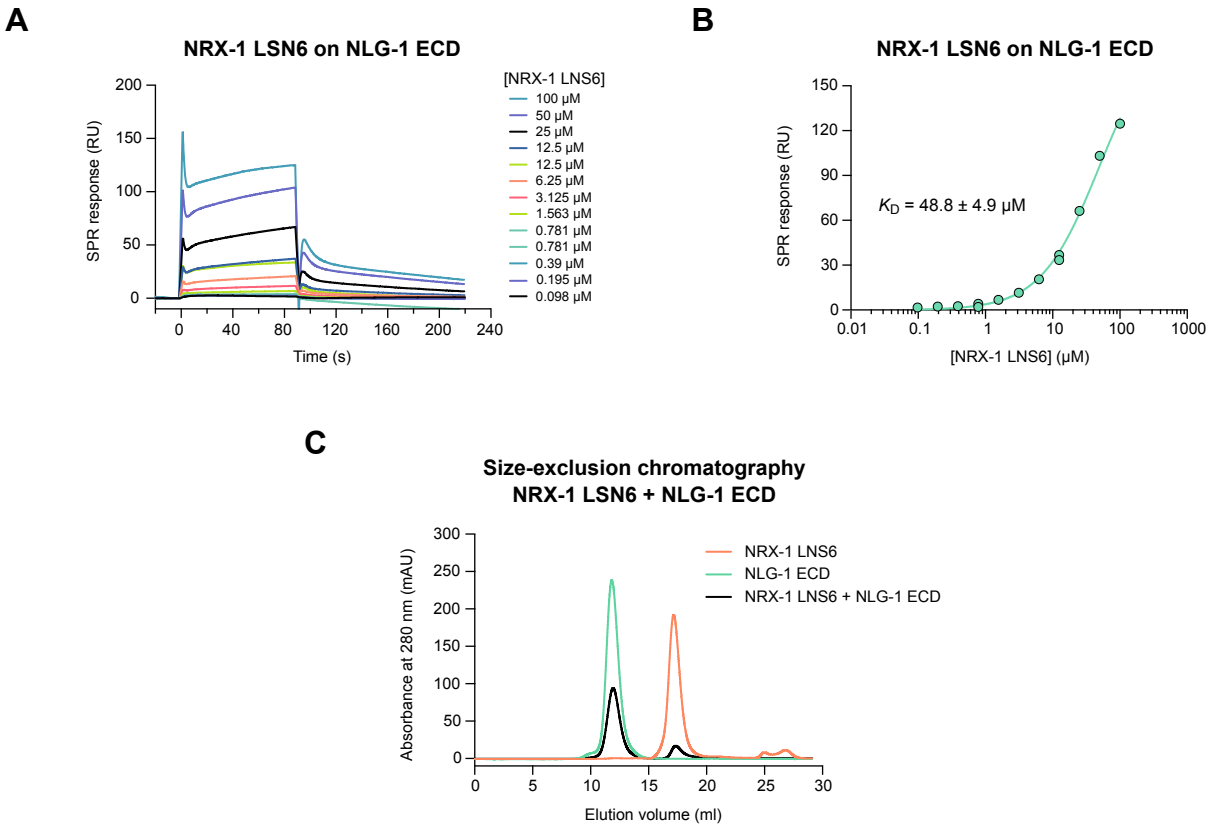

Figure S7. Binding experiments for NLG-1–NRX-1 complex.
A. SPR sensorgrams for soluble NRX-1 LNS6 domain binding to immobilized NLG-1 ECD.
B. Binding isotherm and K_D for binding shown in A.
C. Size-exclusion chromatography runs for NRX-1 LNS-6 (orange), NLG-1 ECD (green) and the mixed sample (black).

Table S5. Data and refinement statistics for x-ray crystallography of the ZIG-4–INS-6 complex.

	Tetragonal form	***C*-centered monoclinic**	**Primitive monoclinic**
Data Collection			
Beamline	APS 24-ID-E	APS 24-ID-E	APS 24-ID-E
Space Group	$P4_22_12$	$C2$	$P2_1$
Cell Dimensions			
a, *b*, *c* (Å)	74.528, 74.528, 107.058	166.430, 56.654, 73.685	73.839, 55.739, 149.945
α, β, γ (°)	90, 90, 90	90, 113.247, 90	90, 93.775, 90
Resolution (Å)*	200-1.30 (1.38-1.30)	200-2.30 (2.44-2.30)	200-2.35 (2.49-2.35)
R_{sym} (%)	4.6 (120.1)	7.1 (113.1)	6.2 (124.8)
$\langle I \rangle / \langle \sigma(I) \rangle$	24.0 (1.78)	9.7 (1.1)	10.7 (0.9)
$CC_{1/2}$	0.999 (0.742)	0.998 (0.652)	0.998 (0.463)
Completeness (%)	99.8 (99.4)	98.4 (96.7)	97.9 (97.1)
Redundancy	12.8 (12.2)	3.4 (3.3)	3.1 (3.1)
Refinement			
Resolution (Å)*	50-1.30 (1.32-1.30)	53.13-2.30 (2.38-2.30)	74.81-2.35 (2.60-2.50)
Reflections	73,784	27,969	50,096
R_{cryst} (%)	14.47 (27.19)	21.52 (43.52)	19.66 (38.72)
R_{free} (%)**	16.89 (31.58)	25.18 (47.21)	23.98 (44.33)
Number of atoms			
Protein	2,128	3,878	7,755
Ligand/Glycans	11	0	0
Water	305	7	39
Average B-factors (Å^2)			
All	24.8	76.2	83.1
Protein	23.0	76.3	83.2
Ligand	36.3	N/A	N/A
Solvent	37.0	60.2	57.5
R.m.s. deviations from ideality			
Bond Lengths (Å)	0.012	0.003	0.008
Bond Angles (°)	1.291	0.631	1.002
Ramachandran plot			
Favored (%)	98.41	96.67	97.24
Outliers (%)	0.40	0.00	0.00
Rotamer Outliers (%)	0.43	0.48	0.39
All-atom Clashscore‡	3.34	3.31	3.91

* The values in parentheses are for reflections in the highest resolution bin.
** 5% of reflections (3,747) for tetragonal crystals, 5% of reflections (1,373) for *C*-centered monoclinic crystals, and 4% of reflections (1,977) for primitive monoclinic crystals were not used during refinement for cross validation purposes.
‡ Clashscores were calculated by *phenix.refine* (*Phenix* version 1.21).
N/A: Not applicable.